DOI: 10.1002/ejic.201100612

# Properties of Metal Complexes of a New Dioxadiaza Macrocycle Containing a Dibenzofuran Unit and Acetate Pendant Arms

**Pedro Mateus,[a] Feng Li,[a][‡] Catarina V. Esteves,[a] Rita Delgado,*[a,b] Paula Brandão,[c] and Vítor Félix[d]**

**Keywords:** Macrocyclic ligands / Crown compounds / Aza crown ethers / Heavy metals / Stability constants / N,O ligands / Environmental chemistry

A new dioxadiaza macrocycle containing a rigid dibenzofuran group (DBF) and bearing two acetate pendant arms, $ac_2[17](DBF)N_2O_2$, has been synthesized in good yield by condensation of the parent macrocycle with potassium bromoacetate in basic aqueous solution. The protonation constants of $ac_2[17](DBF)N_2O_2$ and the stability constants of its complexes with $Mn^{2+}$, $Ni^{2+}$, $Cu^{2+}$, $Zn^{2+}$, $Cd^{2+}$ and $Pb^{2+}$ ions were determined at 298.2 K in aqueous solutions and at ionic strength 0.10 mol dm$^{-3}$ in $NMe_4NO_3$. The stability constants revealed that $ac_2[17](DBF)N_2O_2$ has a higher affinity for larger metal ions, $Cd^{2+}$ and $Pb^{2+}$, showing a clear preference for cadmium. Spectroscopic data in solution and X-ray crystal structure determinations revealed that the higher affinity for $Cd^{2+}$ and $Pb^{2+}$ is due to the better fit of these metal ions into the macrocyclic cavity, derived from its ring size and rigidity and the involvement of all the donor atoms of the ligand in the coordination to these metal centres. Considering the negative effect of these heavy metal ions on human health and the environment, this study represents an important step in the development of selective chelators for these two pollutants.

## Introduction

Large quantities of heavy metals have been released into the environment as a consequence of industrial activity, causing damage to ecosystems and negatively affecting human health. Not surprisingly, a large number of scientists from different areas of research have been developing new and improved methods for the treatment of such metal pollution.[1]

Clearly, efficient complexing agents for lead(II), cadmium(II) and mercury(II) may have important applications as selective extractants and as sensors for the detection of these toxic metal ions in solution. In this regard, macrocyclic ligands have been extensively studied.[2–6] Indeed, the macrocyclic framework can be adjusted by changing the number, nature and location of donor atoms, the cavity size and conformational flexibility, allowing the design of highly preorganized ligands with the ability to recognize and selectively bind certain metal ions. In particular, aza crown ethers have shown complexation properties that are between those of all-oxygen crowns, which have a strong affinity for alkali and alkaline earth metal ions, and those of all-nitrogen macrocycles, which strongly complex transition and heavy-metal cations.[7] In addition, a variety of functional pendant sidearms can be attached to unsaturated nitrogen donor atoms in the macrocyclic framework, which further enhances selectivity and thermodynamic stability.[8–11]

Herein a new dioxadiaza macrocyclic ligand containing a rigid dibenzofuran group (DBF) and bearing two acetate pendant arms, $ac_2[17](DBF)N_2O_2$, is presented. This com-

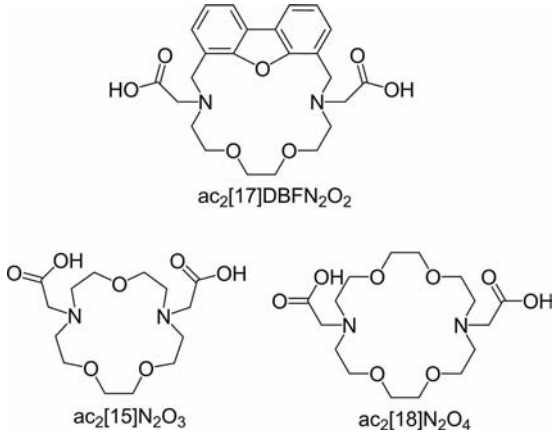


Scheme 1. Structures of the compounds discussed in this work.

[a] Instituto de Tecnologia Química e Biológica, UNL, Av. da República – EAN, 2780-157 Oeiras, Portugal
Fax: +351-21-441-1277
E-mail: delgado@itqb.unl.pt
[b] Instituto Superior Técnico, DEQB, Av. Rovisco Pais, 1049-001 Lisboa, Portugal
[c] Departamento de Química, CICECO, Universidade de Aveiro, 3810-193 Aveiro, Portugal
[d] Departamento de Química, CICECO and Secção Autónoma de Ciências da Saúde, Universidade de Aveiro, 3810-193 Aveiro, Portugal
[‡] Present address: School of Chemistry, University of Sydney, Sydney, NSW 2006, Australia

pound is structurally similar to two previously reported compounds, $ac_2[15]N_2O_3$ and $ac_2[18]N_2O_4$ (Scheme 1).[12,13] However, the dibenzofuran unit is intended to impart more rigidity on the macrocyclic framework in addition to providing a cavity size that is between those of $ac_2[15]N_2O_3$ and $ac_2[18]N_2O_4$. Moreover, the DBF unit should allow the compound to be more lipophilic than those with only aliphatic chains, an important feature for extraction applications.[14]

## Results and Discussion

### Synthesis of $ac_2[17](DBF)N_2O_2$

The compound $ac_2[17](DBF)N_2O_2$ was prepared according to a published procedure,[15] which involves condensation of the parent macrocycle, $[17](DBF)N_2O_2$, with bromoacetate under basic conditions (Scheme 2).

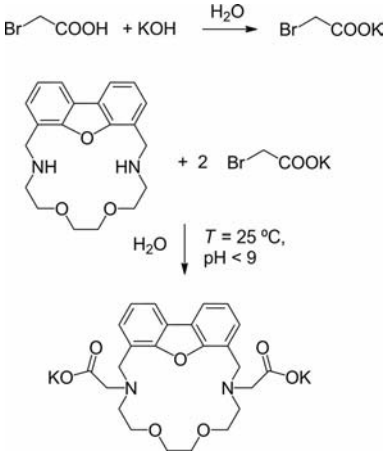


Scheme 2. Synthesis of $ac_2[17](DBF)N_2O_2$.

### Acid–Base Behaviour of $ac_2[17](DBF)N_2O_2$

The acid–base reactions of $ac_2[17](DBF)N_2O_2$ were studied by potentiometry at 298.2 K and 0.10 mol dm$^{-3}$ $NMe_4NO_3$ ionic strength in aqueous solution. The protonation constants are collected in Table 1. The first two protonation constants correspond to the protonation of the tertiary amines of the macrocycle, and they are somewhat lower than those of $ac_2[15]N_2O_3$[16] and $ac_2[18]N_2O_4$,[17] mainly due to the electron withdrawing effect of the DBF group. The remaining constant corresponds to the protonation of one of the carboxylate groups, whereas the other is too low to be determined by potentiometry, as found for the compounds presented for comparison.

Table 1. Stepwise protonation ($K_i^H$) constants of $ac_2[17](DBF)N_2O_2$, $ac_2[15]N_2O_3$ and $ac_2[18]N_2O_4$.[a]

| Equilibrium | $ac_2[17](DBF)N_2O_2$[b] | $ac_2[15]N_2O_3$[c] | $ac_2[18]N_2O_4$[d] |
|---|---|---|---|
| $L^{2-} + H^+ \rightleftarrows HL^-$ | 8.42(1) | 9.07 | 8.93 |
| $HL^- + H^+ \rightleftarrows H_2L$ | 7.66(1) | 8.54 | 8.01 |
| $H_2L + H^+ \rightleftarrows H_3L^+$ | 2.47(1) | 1.75 | 2.50 |
| $L + 3\,H^+ \rightleftarrows H_3L^+$ | 18.55 | 19.35 | 19.44 |

[a] $T = (298.2 \pm 0.1)$ K; $I = (0.10 \pm 0.01)$ mol dm$^{-3}$ in $NMe_4NO_3$. [b] This work. [c] Ref.[16] [d] Ref.[17]

### Metal Complexation Studies

The stability constants of the complexes of $ac_2[17](DBF)N_2O_2$ with $Mn^{2+}$, $Ni^{2+}$, $Cu^{2+}$, $Zn^{2+}$, $Cd^{2+}$ and $Pb^{2+}$ ions were determined by potentiometry at 298.2 K and 0.10 mol dm$^{-3}$ $NMe_4NO_3$ ionic strength in aqueous solution. The results are listed in Table 2.

It was found that $ac_2[17](DBF)N_2O_2$ forms mononuclear $MHL^+$ and ML species in solution with the metal ions studied. Due to precipitation problems at high pH values, it was not possible to determine the stability constants of the hydroxo complexes. The existence of $MHL^+$ species (for M = Ni, Cu and Cd) indicates that at least one of the macrocyclic amines is not coordinated to the metal centre at low pH, which only occurs at slightly higher pH upon adjustment of the macrocycle to the metal centre.

Complexes of $ac_2[17](DBF)N_2O_2$ follow the Irving–Williams order of stability, in contrast to those of $[17](DBF)N_2O_2$,[18] $ac_2[15]N_2O_3$[16] and $ac_2[18]N_2O_4$.[17] The stability constants of the metal complexes of $ac_2[17](DBF)N_2O_2$ are significantly higher than those of the parent macrocycle due to the coordination of the acetate pendant arms (see Table 2). However, identical to $[17](DBF)N_2O_2$, $ac_2[17](DBF)N_2O_2$ exhibits a preference for the larger metal ions $Cd^{2+}$ and $Pb^{2+}$, which means that the selectivity pattern observed is a consequence of the ring size and rigidity of the macrocyclic structure. The stability constants of $[Cd\{ac_2[17](DBF)N_2O_2\}]$ and $[Pb\{ac_2[17](DBF)N_2O_2\}]$ are higher than those for the corresponding $Zn^{2+}$ and $Ni^{2+}$ complexes, which suggests the involvement of all the donor atoms of the ligand in the more stable complexes. Indeed, the single-crystal X-ray diffraction determination of $[Cd\{ac_2[17](DBF)N_2O_2\}]$ (**1**) revealed a good fit of $Cd^{2+}$ into the cavity and the involvement of all the donor atoms of the ligand (see below).

Interestingly, although $ac_2[17](DBF)N_2O_2$ has the same number and approximately the same spatial arrangement of donor atoms as $ac_2[15]N_2O_3$, the stability constants of its metal complexes are much closer to those of $ac_2[18]N_2O_4$, which suggests that the DBF framework not only increases the cavity size relative to $ac_2[15]N_2O_3$ but also imposes an additional strain into the macrocycle, which leads to a different availability of the donor atoms.

Figure 1 illustrates the selectivity trends of $ac_2[15]N_2O_3$, $ac_2[17](DBF)N_2O_2$ and $ac_2[18]N_2O_4$ with their competitive binding diagrams, in which the overall percentages of the complex species as a function of pH are displayed for systems containing the ligand and equimolecular amounts of several metal ions ($Mn^{2+}$, $Ni^{2+}$, $Zn^{2+}$, $Cd^{2+}$ and $Pb^{2+}$). It is interesting to note that as the cavity size increases from $ac_2[15]N_2O_3$ to $ac_2[18]N_2O_4$, binding of larger $Pb^{2+}$ ions becomes favoured. Indeed, $ac_2[15]N_2O_3$ prefers to bind $Zn^{2+}$ (Figure 1, a), whereas $ac_2[17](DBF)N_2O_2$ prefers $Cd^{2+}$ (Fig-

  

Table 2. Stability constants (log *K*) of the complexes of $ac_2[17](DBF)N_2O_2$ with divalent metal ions. Values for the parent macrocycle and related compounds $ac_2[15]N_2O_3$ and $ac_2[18]N_2O_4$ are also presented for comparison.

| Reaction equilibrium[a] | $[17](DBF)N_2O_2$[b] | $ac_2[17](DBF)N_2O_2$[c] | $ac_2[15]N_2O_3$[d] | $ac_2[18]N_2O_4$ |
|---|---|---|---|---|
| $Mn^{2+} + L \rightleftarrows MnL$ | 3.08 | 7.07(1) | 12.11 | 8.65[e] |
| $MnL + H^+ \rightleftarrows MnHL$ | 7.74 | – | – | – |
| $MnLOH + H^+ \rightleftarrows MnL$ | 7.62 | – | – | – |
| $Ni^{2+} + L \rightleftarrows NiL$ | 3.38 | 7.80(1) | 12.37 | 8.56[e] |
| $NiL + H^+ \rightleftarrows NiHL$ | – | 5.09(5) | – | – |
| $NiL + Ni^{2+} \rightleftarrows Ni_2L$ | – | – | 1.93 | 1.94[e] |
| $Cu^{2+} + L \rightleftarrows CuL$ | 6.99 | 14.70(2) | 17.79 | 15.36[e] |
| $CuL + H^+ \rightleftarrows CuHL$ | 6.05 | 2.29(5) | – | – |
| $CuLOH + H^+ \rightleftarrows CuL$ | 7.64 | – | – | – |
| $CuL(OH)_2 + H^+ \rightleftarrows CuLOH$ | 8.88 | – | – | – |
| $CuL + Cu^{2+} \rightleftarrows Cu_2L$ | – | – | 5.00 | 2.52[e] |
| $Zn^{2+} + L \rightleftarrows ZnL$ | 3.46 | 8.72(1) | 14.44 | 8.96[e] |
| $ZnL + Zn^{2+} \rightleftarrows Zn_2L$ | – | – | 2.91 | 2.14[e] |
| $Cd^{2+} + L \rightleftarrows CdL$ | 5.51 | 10.51(1) | 13.43 | 11.07[f] |
| $CdL + H^+ \rightleftarrows CdHL$ | 5.78 | 3.3(1) | – | – |
| $CdLOH + H^+ \rightleftarrows CdL$ | 9.24 | – | – | – |
| $CdL + Cd^{2+} \rightleftarrows Cd_2L$ | – | – | 2.19 | – |
| $Pb^{2+} + L \rightleftarrows PbL$ | – | 9.82(1) | 13.23 | 13.55[f] |
| $PbL + Pb^{2+} \rightleftarrows Pb_2L$ | – | – | 2.44 | – |

[a] Charges of the ligands and complexes are omitted for simplicity. [b] $T = (298.2 \pm 0.1)$ K; $I = (0.10 \pm 0.01)$ mol dm$^{-3}$ in $KNO_3$ and $H_2O$/MeOH (1:1 v/v). The stepwise protonation constants ($K_i^H$) of $[17](DBF)N_2O_2$ are: 8.01, 7.13.[18] [c] $T = (298.2 \pm 0.1)$ K; $I = (0.10 \pm 0.01)$ mol dm$^{-3}$ in aqueous $NMe_4NO_3$. This work. [d] $T = (298.2 \pm 0.1)$ K; $I = (0.10 \pm 0.01)$ mol dm$^{-3}$ in aqueous $NMe_4NO_3$.[16] [e] $T = (298.2 \pm 0.1)$ K; $I = (0.10 \pm 0.01)$ mol dm$^{-3}$ in aqueous $NMe_4NO_3$.[17] [f] $T = (298.2 \pm 0.1)$ K; $I = (0.10 \pm 0.01)$ mol dm$^{-3}$ in aqueous $NMe_4Cl$.[19]

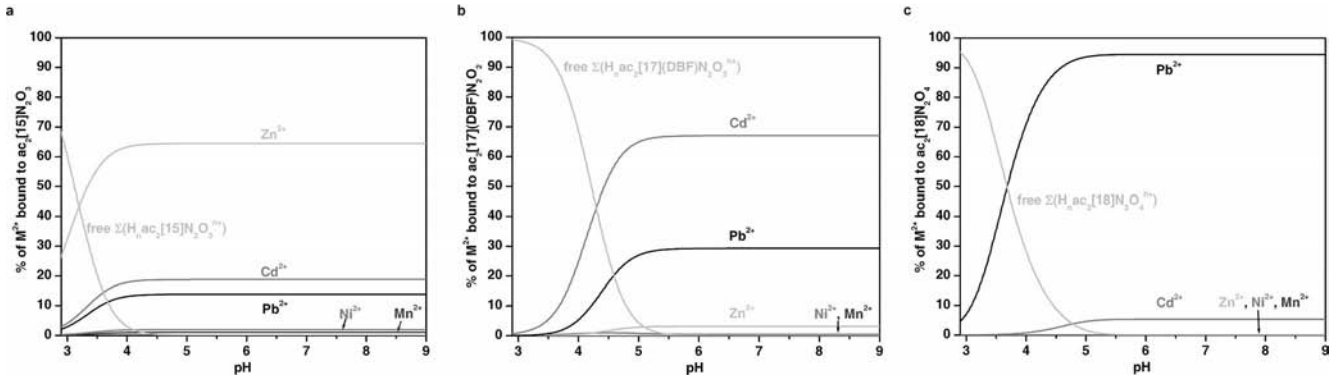


Figure 1. Distribution diagrams of the overall amounts of complex species formed between $ac_2[15]N_2O_3$ (a), $ac_2[17](DBF)N_2O_2$ (b) and $ac_2[18]N_2O_4$ (c) and each metal ion. Where $Mn^{2+}$, $Ni^{2+}$, $Zn^{2+}$, $Cd^{2+}$ and $Pb^{2+}$ represent the corresponding metal in all complex forms $\Sigma[(M)(H_nL)]$, where L is the ligand and M the metal ion. $C_L = C_M = 1.0 \times 10^{-3}$ mol dm$^{-3}$.

ure 1, b) and $ac_2[18]N_2O_4$ prefers $Pb^{2+}$ (Figure 1, c) from a mixture of $Mn^{2+}$, $Ni^{2+}$, $Zn^{2+}$, $Cd^{2+}$ and $Pb^{2+}$ in aqueous solution (pH > 5).

Although a few macrocyclic compounds with affinity for cadmium and lead that show selectivity for these metal ions in relation to zinc in aqueous solution have been reported,[3,20–23] the series of compounds with identical donor atoms and the same pendant arms described here is the only case where it was possible to demonstrate the change of selectivity from zinc(II) to lead(II) by the gradual increase in cavity size.

## Structural Studies

### UV/Vis/NIR Spectra in Solution

The UV/Vis/NIR spectra of the nickel(II) and copper(II) complexes of $ac_2[17](DBF)N_2O_2$ were recorded in aqueous solution at room temperature (Table 3).

The absorption spectrum of the nickel complex exhibits three low-intensity bands at 940, 628 and 362 nm and several shoulders. This spectrum is characteristic of $d^8$ configuration in distorted octahedral symmetry, corresponding to

  

Table 3. Spectroscopic UV/Vis/NIR data for the complexes of $Ni^{2+}$ and $Cu^{2+}$ with $ac_2[17](DBF)N_2O_2$ in aqueous solution at room temperature.

| Complex | pH | UV/Vis/NIR $\lambda_{max}$ [nm] ($\varepsilon_{molar}$ [$dm^3 mol^{-1} cm^{-1}$]) |
|---|---|---|
| [Ni{$ac_2$[17](DBF)$N_2O_2$}] | 7.5 | 202 ($2.8\times10^5$), 244 ($9.9\times10^3$), 252 ($10^4$), 282 ($9.4\times10^3$), 286 (sh, $7.3\times10^3$), 292 (sh, $5.9\times10^3$), 298 (sh, $3.9\times10^3$), 305 (sh, $1.4\times10^3$), 362 (74), 628 (5), 675 (sh, 4), 940 (3) |
| [Cu{$ac_2$[17](DBF)$N_2O_2$}] | 5.0 | 202 ($5.6\times10^5$), 254 ($8.8\times10^3$), 282 ($8.3\times10^3$), 288 (sh, $5.9\times10^3$), 295 (sh, $5.0\times10^3$), 307 (sh, $4.1\times10^3$), 308 (sh, $2.3\times10^3$), 660 (31), 767 (sh, 22) |

the three spin allowed transitions from $3A_{2g}$ to $3T_{2g}$, $3T_{1g}$ and $3T_{1g}(P)$.[24] The copper(II) complex of $ac_2[17](DBF)N_2O_2$ exhibits a broad asymmetric band in the visible region at 660 nm tailing into the NIR region, due to the copper d–d transition. The EPR spectrum of this complex (Figure 2) exhibits four well resolved lines at low field due to the interaction of the unpaired electron spin with the copper nucleus, and no superhyperfine splitting due to coupling with the nitrogen atoms of the macrocycle. The simulation of the spectrum indicated three different principal values of $g$, $g_1 > (g_2 + g_3)/2$ and the lowest $g > 2.04$, typical of rhombic symmetry of $Cu^{2+}$ with elongation of the axial bonds and a $d_{x^2-y^2}$ ground state. Elongated rhombic octahedral, rhombic square coplanar or distorted square-based pyramidal geometries would be consistent with these data. The hyperfine coupling constants and $g$ values are compiled in Table 4.

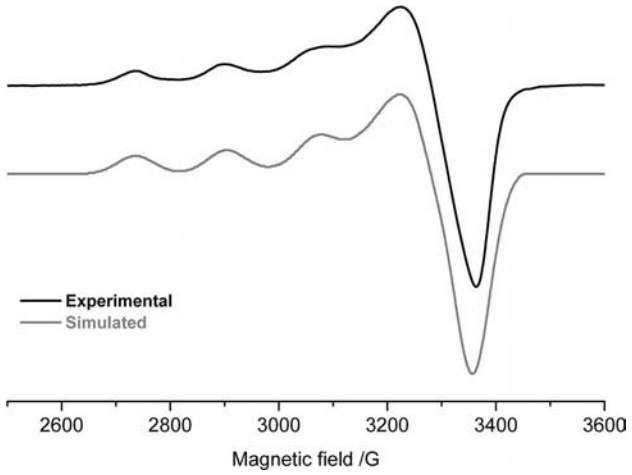


Figure 2. Experimental and simulated X-band EPR spectrum of the copper(II) complex of $ac_2[17](DBF)N_2O_2$ in 1.0 mol $dm^{-3}$ $NaClO_4$, recorded at 90 K, microwave power 2.0 mW, frequency ($\nu$) 9.495 GHz.

As no superhyperfine splitting was found, Blumberg–Peisach plots,[25] which correlate $g_\parallel$ and $A_\parallel$ with equatorial coordination spheres, were used to identify the donor atoms coordinated to $Cu^{2+}$ ion. The $g_\parallel$ and $A_\parallel$ values for the $Cu^{2+}$ centre in [Cu{$ac_2$[17](DBF)$N_2O_2$}] indicate a neutral [Cu($N_2O_2$)] complex, which suggests that the equatorial plane is made up of the two nitrogen atoms of the macrocycle and two oxygen atoms of the acetate arms, whereas the oxygen atom of the dibenzofuran unit and one of the two ether oxygen atoms of the macrocycle are the two axial ligands.

Table 4. The hyperfine coupling constants and $g$ values taken from the simulation of the X-band EPR spectrum of the copper(II) complex of $ac_2[17](DBF)N_2O_2$.[a]

| Complex | $g_1$ | $g_2$ | $g_3$ | $A_1$ $\times 10^4$ $cm^{-1}$ | $A_2$ | $A_3$ |
|---|---|---|---|---|---|---|
| [Cu{$ac_2$[17](DBF)$N_2O_2$}] | 2.272 | 2.081 | 2.063 | 177 | 38 | 2 |

[a] 1.0 mol $dm^{-3}$ $NaClO_4$ aqueous solution, recorded at 90 K, microwave power 2.0 mW, frequency 9.495 GHz.

## Single-Crystal X-Ray Structures of $Cd^{2+}$ and $Ni^{2+}$ Complexes

The asymmetric unit of the $Cd^{2+}$ complex **1** contains one molecule of [Cd{$ac_2$[17](DBF)$N_2O_2$}] and four water molecules giving the molecular formula [Cd{$ac_2$[17](DBF)$N_2O_2$}]·$4H_2O$. The asymmetric unit of the $Ni^{2+}$ complex is composed of two independent [Ni{$ac_2$[17](DBF)$N_2O_2$}] units and four crystallization water molecules, which is consistent with the molecular formula [Ni{$ac_2$[17](DBF)$N_2O_2$}]·$2H_2O$ (**2**). Selected bond lengths and angles for **1** and **2** are given in Table 5.

Table 5. Bond lengths [Å] and angles [°] for **1** and **2**.

| | **1** | **2** | |
|---|---|---|---|
| | | **A** | **B** |
| M–O(8) | 2.544(2) | 2.184(5) | 2.168(5) |
| M–O(19) | 2.258(2) | 1.986(5) | 1.963(5) |
| M–O(23) | 2.474(2) | 2.314(8) | 2.497(6) |
| M–O(26) | 2.408(2) | – | – |
| M–O(32) | 2.217(2) | 1.982(5) | 1.985(5) |
| M–N(16) | 2.347(2) | 2.109(6) | 2.117(6) |
| M–N(29) | 2.377(2) | 2.134(6) | 2.122(6) |
| O(8)–M–O(23) | 137.75(6) | 166.6(3) | 153.6(2) |
| O(23)–M–O(26) | 67.80(6) | – | – |
| O(26)–M–N(29) | 74.31(7) | – | – |
| O(8)–M–O(26) | 67.80(6) | – | – |
| O(8)–M–N(29) | 79.27(6) | 85.7(2) | 89.6(2) |
| O(8)–M–N(16) | 74.06(6) | 86.4(2) | 84.2(2) |
| N(16)–M–O(23) | 75.26(7) | 80.3(3) | 78.0(2) |
| O(32)–M–O(19) | 168.11(7) | 176.9(2) | 174.0(2) |
| N(16)–M–N(29) | 149.80(7) | 171.3(3) | 169.4(2) |

The ORTEP view of **1** (Figure 3) shows the cadmium centre encapsulated by $ac_2[17](DBF)N_2O_2$ in a distorted pentagonal bipyramid geometry. The equatorial [$N_2O_3$] coordination plane is determined by the backbone macrocyclic atoms with the *cis* N–Cd–O angles ranging from 74.06(6)–79.27(6)° and an O(26)–Cd–O(23) angle of 67.80(6)°. The coordination number of seven is achieved by coordination of oxygen atoms O(32) and O(19) of the carboxylate pendant arms, which make an angle with the cadmium centre deviated 11.99(7)° from the ideal (180°).

  

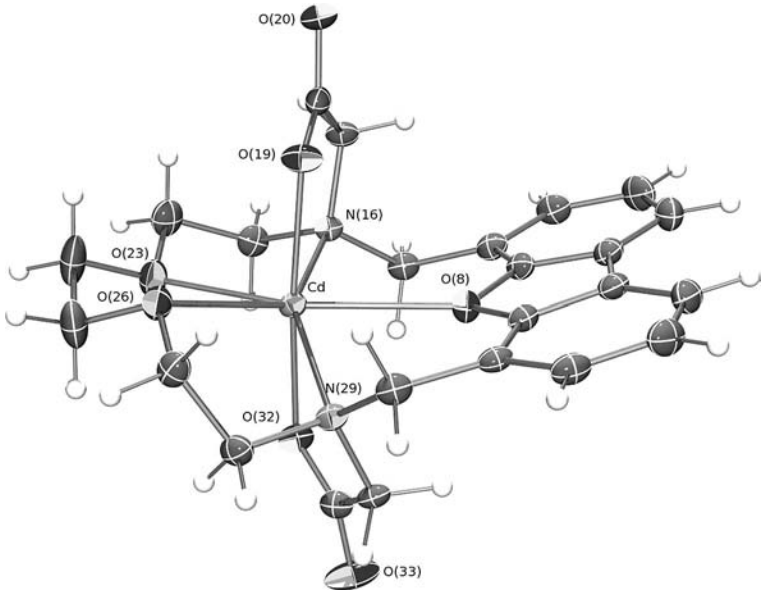


Figure 3. ORTEP view of **1** (ellipsoids drawn at 50% probability), which shows the overall structure and the labelling scheme.

The Cu–O distance to the DBF aromatic moiety [2.544(2) Å] is ca. 0.1 Å longer than the distances to the ether oxygen donors [2.474(2) and 2.408(2) Å], whereas the Cd–N distances of 2.347(2) and 2.377(2) Å are comparable. The cadmium ion is out of the plane defined by the equatorial donor atoms by 0.07(1) Å. These two structural features indicate that there is enough room to accommodate large ions such as $Cd^{2+}$ in the macrocyclic cavity.

Figure 4 shows an ORTEP diagram of one of two crystallographically independent molecules (**B**) of **2**. In **B**, the aliphatic $–NCH_2CH_2OCH_2CH_2–$ linkage is disordered over two positions (see Exp. Sect.) giving rise to two slightly different conformations for the macrocyclic backbone. **A** and **B** display equivalent bond lengths and angles subtended at the nickel centre with the exception of the Ni–O(23) distance, which is 2.314(8) and 2.497(6) Å in **A** and **B**, respectively. The metal centre is inserted into the $ac_2$[17](DBF)-$N_2O_2$ cavity in a distorted octahedral geometry with the $[N_2O_2]$ equatorial coordination plane defined by the macrocyclic backbone atoms O(8), O(23), N(16) and N(29). In contrast with that observed in **1**, the disordered oxygen atom O(26) is away from the nickel centre at distance of 3.442(2) Å in **A** and 3.454(8) Å in **B**. In both molecules, the Ni–O and Ni–N distances are similar and are within the range of expected values for $Ni^{II}$ octahedral complexes.[26] This is also true of the *cis* angles on the equatorial coordination plane, which range between 80.3(3) and 86.4(2)° for **A** and 78.0(2) and 89.6(2)° for **B**. The $O_{axial}$–Ni–$O_{axial}$ angle is slightly deviated from the ideal by 3.1(2)° in **A** and 6.0(2)° in **B**.

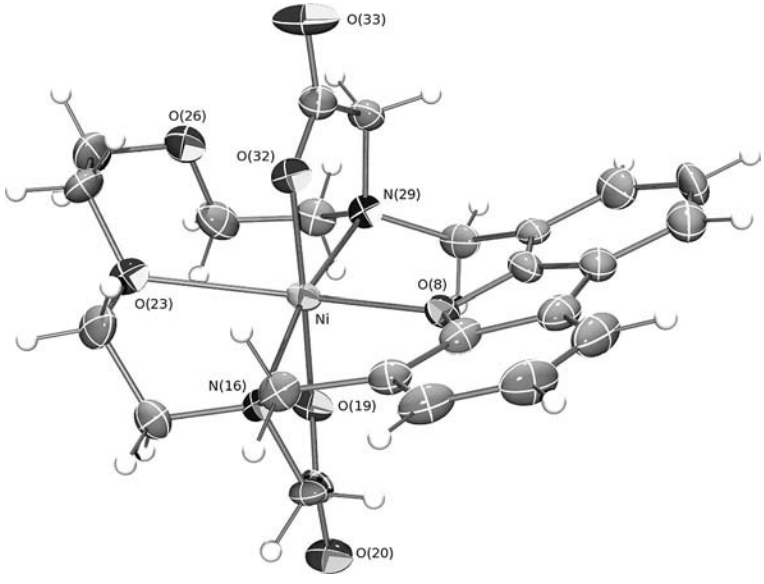


Figure 4. ORTEP view of one of the two independent molecules of **2** (molecule **B**). Thermal ellipsoids are drawn at 50% probability.

  

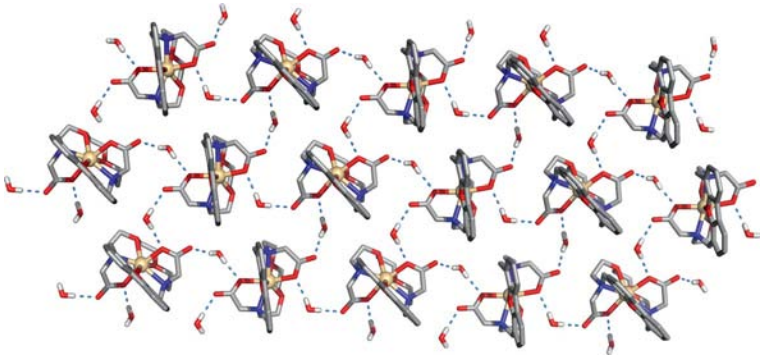

Figure 5. Crystal packing diagram of **1** showing the 2D network of O–H···O hydrogen bonds, which are drawn as dashed lines. C–H hydrogen atoms are omitted for clarity.

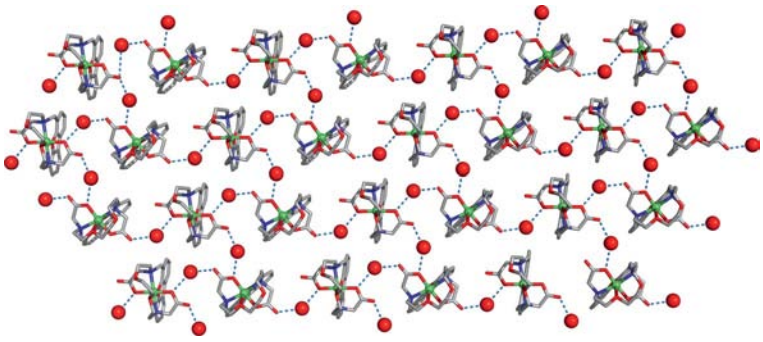

Figure 6. Crystal packing diagram of **2** showing the 2D network of O–H···O hydrogen bonds, which are drawn as dashed lines. C–H hydrogen atoms are omitted for clarity.

A detailed analysis of the hydrogen bonding interactions in both complexes is limited by the absence of the hydrogen atoms from all water molecules in **2** and from the disordered one in **1** (see below). However, the O···O distances found between the metal complexes and crystallization water molecules show that in both cases a 2D O–H···O network of hydrogen bonds are formed (see Figures 5 and 6). In **1**, the network grows up from a centrosymmetric ring motif composed of four water and four complex molecules with O···O distances ranging from 1.96(2)–2.05(2) Å and O–H···O angles between 163(3) and 178(4)°. In **2**, there is also a large macrocyclic central motif formed by six water molecules and six nickel complexes assembled by hydrogen bonds with O···O distances between 2.78(1) and 2.89(3) Å.

## Conclusions

A *N*,*N*-bis(carboxymethyl) derivative of [17](DBF)$N_2O_2$, $ac_2$[17](DBF)$N_2O_2$, was synthesized in good yield for the first time. The DBF moiety, besides rigidifying the macrocyclic framework, allowed the construction of a cavity size intermediate of those of $ac_2$[15]$N_2O_3$ and $ac_2$[18]$N_2O_4$. It was clearly shown from an aqueous solution containing equimolar amounts of $Mn^{2+}$, $Ni^{2+}$, $Zn^{2+}$, $Cd^{2+}$ and $Pb^{2+}$ ions that the three macrocycles prefer the larger $Zn^{2+}$, $Cd^{2+}$ and $Pb^{2+}$ ions but their selectivity pattern differs. Although $ac_2$[15]$N_2O_3$ exhibits a preference for $Zn^{2+}$, $ac_2$[17](DBF)-$N_2O_2$ shows higher affinity for $Cd^{2+}$ followed by $Pb^{2+}$. In turn, $ac_2$[18]$N_2O_4$ preferably coordinates $Pb^{2+}$.

The single-crystal X-ray diffraction determination of [Cd{$ac_2$[17](DBF)$N_2O_2$}] (**1**) and [Ni{$ac_2$[17](DBF)$N_2O_2$}] (**2**) corroborated the conclusion made from the solution studies (potentiometric and spectroscopic) that the higher thermodynamic stability of **1** and [Pb{$ac_2$[17](DBF)$N_2O_2$}] relative to **2** and [Zn{$ac_2$[17](DBF)$N_2O_2$}] stems from the involvement of all the donor atoms of the ligand in the coordination to the metal centre in the more stable complexes, whereas in the less stable complexes at least one oxygen atom of the macrocycle is not coordinated to the metal centre.

It was shown that the unusual selectivity for $Cd^{2+}$ and $Pb^{2+}$ exhibited by $ac_2$[17](DBF)$N_2O_2$ is governed by the ring size and the rigidity of the macrocycle. Considering the damage that these metal ions cause to the environment and their negative effect in human health, this study represents an important step in the development of selective chelators for these two pollutants.

## Experimental Section

**General Considerations:** The parent macrocycle [17](DBF)$N_2O_2$ was prepared as reported.[27] All solvents and chemicals were purchased as reagent grade quality and used as supplied without fur-

  

ther purification. NMR spectra used for characterization of products were recorded with a Bruker Avance 400 instrument. Peak assignments are based on peak integration and multiplicity for 1D $^1$H spectra and COSY, NOESY and HMQC experiments. Microanalyses were carried out by the ITQB Microanalytical Service. The absorption spectra were recorded with a UNICAM UV/Vis spectrophotometer model UV-4 (in the UV/Vis range) and Shimadzu model UV-3100 spectrophotometer (in the NIR range). EPR spectroscopy measurements were recorded with a Bruker ESP 380 spectrometer equipped with continuous flow cryostat for liquid nitrogen operating at X-band.

### Syntheses

**ac$_2$[17](DBF)N$_2$O$_2$:** ac$_2$[17](DBF)N$_2$O$_2$ was prepared by condensation of the parent macrocycle [17](DBF)N$_2$O$_2$ (1.2 mmol, 408 mg) with potassium bromoacetate (obtained by addition of 3 mol dm$^{-3}$ KOH solution to concentrated aqueous bromoacetic acid, 2.64 mmol, 368 mg) in basic aqueous solution. The temperature was kept at 25–30 °C and the pH below 9 by slow addition of 3 mol dm$^{-3}$ KOH. The reaction was considered complete after 7 d and the pH was adjusted to 2 with 3 mol dm$^{-3}$ HCl. The product was purified by chromatography using a cationic resin Amberlite CG-50 in the H$^+$ form. The fractions containing the pure compound were combined and evaporated to yield a yellow solid, which was washed several times with water and dried under vacuum; yield 301 mg (55%); m.p. 92 °C (decomp.). $^1$H NMR (400 MHz, $CDCl_3$, 298 K, $Me_4Si$): $\delta$ = 3.44 (m, 8 H, NC$H_2$CH$_2$O and OC$H_2$C$H_2$O), 3.68 (m, 4 H, NCH$_2$C$H_2$O), 4.02 (s, 4 H, NC$H_2$COOH), 4.42 (s, 4 H, DBFC$H_2$N), 7.25 [t, 2 H, $^3J$(H,H) = 7.6 Hz, DBF], 7.38 [d, 2 H, $^3J$ (H,H) = 7.2 Hz, DBF], 7.84 [d, 2 H, $^3J$(H,H) = 7.6 Hz, DBF] ppm. $^{13}$C NMR (100 MHz, $CDCl_3$, 298 K, $Me_4Si$): $\delta$ = 53.37 (DBF*C*H$_2$N), 53.78 (N*C*H$_2$COOH), 54.41 (N*C*H$_2$CH$_2$O), 63.58 (NCH$_2$*C*H$_2$OCH$_2$), 69.72 (NCH$_2$CH$_2$O*C*H$_2$), 112.3, 123.74, 124.2, 130.9, 153.97 (DBF) and 167.91 (COOH) ppm. $C_{24}H_{28}N_2O_7\cdot H_2O$ (474.20): calcd. C 60.75, H 6.37, N 5.90; found C 60.83, H 6.49, N 5.66%. ESI-MS (MeOH): $m/z$ = 457.2 [M + H]$^+$.

**[Cd{ac$_2$[17](DBF)N$_2$O$_2$}] (1) and [Ni{ac$_2$[17](DBF)N$_2$O$_2$}] (2):** ac$_2$[17](DBF)N$_2$O$_2$ (4.6 mg, 10 μmol) was dissolved in water (0.30 mL) and M(NO$_3$)$_2$ (M = Ni or Cd, 0.200 mL, 0.05 mol dm$^{-3}$) was added. The pH was adjusted to 7.5 for the nickel(II) complex solution and to 7.0 for that of cadmium(II) with $NMe_4OH$. The solution was evaporated to dryness, dissolved in MeOH (0.300 cm$^3$) and allowed to crystallize by slow evaporation. Single colourless crystals suitable for X-ray crystallographic determination were obtained within three days.

### Potentiometric Measurements

**Reagents and Solutions:** All the solutions were prepared using demineralised water (obtained by a Millipore/Milli-Q system). A stock solution of the ligand was prepared at ca. $2.0\times10^{-3}$ mol dm$^{-3}$. The $NMe_4NO_3$ salt was prepared by neutralization of commercial $NMe_4OH$ solution with $HNO_3$ and recrystallized from 80% ethanol. Carbonate-free solutions of the titrant $NMe_4OH$ were obtained at ca. 0.10 mol dm$^{-3}$ by treating freshly prepared silver oxide with a solution $NMe_4I$ under a nitrogen atmosphere according to the method of Schwarzenbach and Biederman.[28] These solutions were discarded every time carbonate concentration was about 0.5% of the total amount of base. The titrant solutions were standardized (tested by Gran's method).[29] For the back titrations, a 0.100 mol dm$^{-3}$ standard solution of $HNO_3$ was prepared by dilution of a commercial ampoule. Stock solutions of the metal salts were prepared at about $5.0\times10^{-2}$ mol dm$^{-3}$ from analytical grade nitrate salts and the exact concentration checked by titration with $K_2H_2$edta following standard methods.[30]

**Equipment and Working Conditions:** The equipment used has been described before.[31] The ionic strength of the experimental solutions was kept at $0.10\pm0.01$ mol dm$^{-3}$ with $NMe_4NO_3$, and the temperature was maintained at $298.2\pm0.1$ K. Atmospheric $CO_2$ was excluded from the titration cell during experiments by passing purified nitrogen across the top of the experimental solution.

**Measurements:** The [H$^+$] of the solutions was determined by the measurement of the electromotive force of the cell, $E = E^{\circ\prime} + Q\log[H^+] + E_j$. The term pH is defined as $-\log[H^+]$. $E^{\circ\prime}$, $Q$, $E_j$ and $K_w$ were determined by titration of a solution of known hydrogen ion concentration at the same ionic strength, using the acidic pH range of the titration. The liquid-junction potential, $E_j$, was found to be negligible under the experimental conditions used. The value of $K_w$ was determined from data obtained in the alkaline range of the titration, considering $E^{\circ\prime}$ and $Q$ valid for the entire pH range and found to be equal to $10^{-13.80}$ under our experimental conditions. Before and after each set of titrations, the glass electrode was calibrated as a [H$^+$] probe by titration of $1.0\times10^{-3}$ mol dm$^{-3}$ standard HCl solution with standard KOH. The measurements during the conventional titrations were carried out with ca. 0.040 mmol of the ligand in a total volume of 30.00 mL, both in the absence of the metal ions and in the presence of each metal ion in 1.0 and 2.0 $C_M/C_L$ ratios. Each titration curve typically consisted of one hundred points in the 2.0–10.0 pH range, with a minimum of two replicates undertaken. Back titrations were performed with standard $HNO_3$ solution in order to check if equilibrium had been attained throughout the pH range and to confirm the values of the final $E^{\circ\prime}$ readings.

**Calculation of Equilibrium Constants:** Overall protonation constants, $\beta_i^H$, of the free ligand were calculated by fitting the potentiometric data obtained for all the performed titrations in the same experimental conditions with the HYPERQUAD program.[32] Stability constants of the various species formed in solution were obtained from the experimental data corresponding to the potentiometric titration of solutions of the different metal ions, each with different metal to ligand ratios, also using the HYPERQUAD program. The initial computations were obtained in the form of overall stability constants, $\beta_{M_mH_hL_l} = [M_mH_hL_l]/[M]^m[H]^h[L]^l$. The errors quoted are the standard deviations of the overall stability constants given directly by the program for the input data, which include all the experimental points of all titration curves. The HYSS program[33] was used to calculate the concentration of equilibrium species from the calculated constants from which distribution diagrams were plotted. The species considered in a particular model were those that could be justified by the principles of coordination chemistry.

**Spectroscopic Studies:** Absorption spectra were measured using aqueous solutions of the complexes prepared by the addition of metal ion (in the form of nitrate salts) to the ligand and adjusting to the appropriate pH value by small additions of either standard $NMe_4OH$ or $HNO_3$ solutions. X-band EPR spectroscopic measurements of the copper(II) complex were recorded at concentration of about $4.0\times10^{-3}$ mol dm$^{-3}$ in 1.0 mol dm$^{-3}$ $NaClO_4$. The EPR spectrum was simulated using SpinCount software.[34]

**Crystallography:** The single-crystal X-ray data of **1** and **2** were collected with a CCD Bruker APEX II at 150(2) K using graphite-monochromatized Mo-$K_\alpha$ radiation ($\lambda$ = 0.71073 Å). The selected crystal of each complex was positioned at 35 mm from the CCD and the spots were measured using an appropriate counting time, 10 and 60 s for **1** and **2**, respectively. Data reductions, including a multiscan absorption correction, were carried out using the

  

SAINT-NT from Bruker AXS. Both structures were solved using SHELXS-97[35] and refined on $F^2$ using full-matrix least-squares in SHELXL-97.[36] In **2**, the second molecule of the asymmetric unit was found to be disordered over the macrocyclic backbone. Indeed, the atoms of the $–CH_2OCH_2CH_2–$ fragment were located in two alternative positions, which were introduced in the structure refinement with occupancies of $x$ and $1–x$ being $x$ equal to 0.57(1). Furthermore, these atoms were refined with group isotropic temperature factors and with C–C and C–O distances constrained to 1.54 and 1.44 Å, respectively. Two crystallization water molecules in **1** and one in **2** were also found to be disordered over two close positions, which were inserted in the structure refinement with refined or fixed occupancies. All non-hydrogen atoms, with the exception of those of the $–CH_2OCH_2CH_2–$ fragment of **2**, were refined with anisotropic thermal parameters. The C–H hydrogen atoms were introduced in calculated positions, and the atomic positions of the hydrogen atoms of the two water molecules in **2** were directly obtained from the last difference Fourier maps. The remaining water hydrogen atoms of **2** as well as those for **1** were not discernible from the maps and therefore were not taken into account in the final refinements. All hydrogen atoms were refined with isotropic parameters equivalent to 1.2 times those of the atom to which they were attached. Final $R$ values together with pertinent crystallographic data are summarized in Table 6. The ORTEP views and the crystal packing diagrams presented were drawn with ORTEP-3 and PYMOL, respectively.[37]

Table 6. Crystal data and refinement parameters of **1** and **2**.

| | **1** | **2** |
|---|---|---|
| Empirical formula | $C_{24}H_{34}CdN_2O_{11}$ | $C_{24}H_{30}NiN_2O_9$ |
| $M_w$ | 638.93 | 539.21 |
| Crystal system | monoclinic | triclinic |
| Space group | $P2_1/c$ | $P\bar{1}$ |
| $a$ [Å] | 17.5510(4) | 9.0966(4) |
| $b$ [Å] | 9.2445(2) | 17.2256(6) |
| $c$ [Å] | 17.0348(4) | 17.2914(7) |
| $\alpha$ [°] | 90 | 119.650(2) |
| $\beta$ [°] | 111.2340(10) | 94.159(2) |
| $\gamma$ [°] | 90 | 90.362(2) |
| $V$ [Å$^3$] | 2476.26(10) | 2345.71(16) |
| $Z$ | 4 | 4 |
| $D_c$ [Mg m$^{-3}$] | 1.647 | 1.555 |
| $\mu$ [mm$^{-1}$] | 0.912 | 0.886 |
| Reflections collected | 45403 | 23415 |
| Unique reflections [$R_{int}$] | 4522 [0.0292] | 7984 [0.0405] |
| Final $R$ indices | | |
| $R_1$, $wR_2$ [$I > 2\sigma I$] | 0.0253, 0.0609 [4283] | 0.0861, 0.2066 [4283] |
| $R_1$, $wR_2$ (all data) | 0.0273, 0.0615 | 0.1096, 0.2174 |

CCDC-830289 (for **1**) and -830290 (for **2**) contain the supplementary crystallographic data for this paper. These data can be obtained free of charge from The Cambridge Crystallographic Data Centre via www.ccdc.cam.ac.uk/data_request/cif.

## Acknowledgments

The authors acknowledge FCT, with co-participation of the European Community funds FEDER, POCI, QREN and COMPETE for the financial support under project PTDC/QUI/67175/2006. The NMR spectrometers used in the work are part of the National NMR Network and were purchased in the framework of the National Program for Scientific Re-equipment, contract REDE/1517/RMN/2005, with funds from POCI 2010 (FEDER) and FCT. The authors also thank M. C. Almeida for providing elemental analysis and ESI-MS data from the ITQB Elemental Analysis and Mass Spectrometry Service. P. M. thanks FCT for the grant SFRH/BD/36159/2007.

[1] Y.-S. Ho, M. I. El-Khaiary, in: *Heavy Metals in the Environment - Advances in Industrial and Hazardous Wastes Treatment Series* (Eds.: L. K. Wang, J. P. Chen, Y.-T. Hung, N. K. Shammas), Taylor & Francis Group, CRC Press, New York **2009**, pp. 1–12.
[2] L. F. Lindoy, G. V. Meehan, I. M. Vasilescu, H. J. Kim, J. Lee, S. S. Lee, *Coord. Chem. Rev.* **2010**, *254*, 1713–1725.
[3] C. Bazzicalupi, A. Bencini, S. Biagini, A. Bianchi, E. Faggi, C. Giorgi, M. Marchetta, F. Totti, B. Valtancoli, *Chem. Eur. J.* **2009**, *15*, 8049–8063.
[4] B. P. Hay, R. D. Hancock, *Coord. Chem. Rev.* **2001**, *212*, 61–78.
[5] R. M. Izatt, K. Pawlak, J. S. Bradshaw, R. L. Bruening, *Chem. Rev.* **1995**, *95*, 2529–2586.
[6] R. M. Izatt, K. Pawlak, J. S. Bradshaw, *Chem. Rev.* **1991**, *91*, 1721–2085.
[7] K. Krakowiak, J. S. Bradshaw, D. J. Zamecka-Krakowiak, *Chem. Rev.* **1989**, *89*, 929–972.
[8] R. E. Mewis, S. J. Archibald, *Coord. Chem. Rev.* **2010**, *254*, 1686–1712.
[9] R. D. Hancock, A. E. Martell, *Chem. Rev.* **1989**, *89*, 1875–1914.
[10] T. A. Kaden, *Top. Curr. Chem.* **1984**, *121*, 157–179.
[11] K. P. Wainwright, *Coord. Chem. Rev.* **1997**, *166*, 35–90.
[12] S. Kulstad, L. A. Malmsten, *Acta Chem. Scand., Ser. B* **1979**, *33*, 469–474.
[13] C. A. Chang, M. E. Rowland, *Inorg. Chem.* **1983**, *22*, 3866–3869.
[14] A. T. Yordanov, D. M. Roundhill, *Coord. Chem. Rev.* **1998**, *170*, 93–124.
[15] J. Costa, R. Delgado, M. C. Figueira, R. T. Henriques, M. Teixeira, *J. Chem. Soc., Dalton Trans.* **1996**, 65–73.
[16] R. Delgado, J. J. R. F. da Silva, M. C. T. A. Vaz, *Polyhedron* **1987**, *6*, 29–38.
[17] R. Delgado, J. J. R. F. da Silva, M. C. T. A. Vaz, P. Paoletti, M. Micheloni, *J. Chem. Soc., Dalton Trans.* **1989**, 133–137.
[18] F. Li, R. Delgado, M. G. B. Drew, V. Félix, *Dalton Trans.* **2006**, 5396–5403.
[19] C. A. Chang, M. E. Rowland, *Inorg. Chem.* **1983**, *22*, 3866–3869.
[20] J.-M. Lehn, F. Montavon, *Helv. Chim. Acta* **1978**, *61*, 67–82.
[21] K. V. Damu, M. S. Shaikjee, J. P. Michael, A. S. Howard, R. D. Hancock, *Inorg. Chem.* **1986**, *25*, 3879–3886.
[22] A. Bianchi, M. Micheloni, P. Paoletti, *Coord. Chem. Rev.* **1991**, *110*, 17–113.
[23] J. Costa, R. Delgado, M. G. B. Drew, V. Félix, *J. Chem. Soc., Dalton Trans.* **1999**, 4331–4339.
[24] G. L. Miessler, D. A. Tarr, *Inorganic Chemistry*, 3rd ed., Prentiss Hall, New Jersey, **2003**.
[25] J. Peisach, W. E. Blumberg, *Arch. Biochem. Biophys.* **1974**, *165*, 691–708.
[26] F. H. Allen, *Acta Crystallogr., Sect. B* **2002**, *58*, 380–388.
[27] F. Li, R. Delgado, A. Coelho, M. G. B. Drew, V. Félix, *Tetrahedron* **2006**, *62*, 8550–8558.
[28] G. Schwarzenbach, W. Biederman, *Helv. Chim. Acta* **1948**, *31*, 311–340.
[29] F. J. Rossotti, H. J. Rossotti, *J. Chem. Educ.* **1965**, *42*, 375–378.
[30] G. Schwarzenbach, W. Flaschka, *Complexometric Titrations*, Methuen & Co, London, **1969**.
[31] P. Mateus, R. Delgado, P. Brandão, S. Carvalho, V. Félix, *Org. Biomol. Chem.* **2009**, *7*, 4661–4637.
[32] P. Gans, A. Sabatini, A. Vacca, *Talanta* **1996**, *43*, 1739–1753.

  

[33] L. Alderighi, P. Gans, A. Ienco, D. Peters, A. Sabatini, A. Vacca, *Coord. Chem. Rev.* **1999**, *184*, 311–318.
[34] SpinCount is a Microsoft Windows® software package, which allows quantitative interpretation and simulation of EPR spectra, created by Prof. M. P. Hendrich at Carnegie Mellon University. SpinCount is available on the internet: http://www.chem.cmu.edu/groups/hendrich/.
[35] G. M. Sheldrick, *Acta Crystallogr., Sect. A* **2008**, *64*, 112–122.
[36] L. J. Farrugia, *J. Appl. Crystallogr.* **1997**, *30*, 565–566.
[37] W. L. DeLano, *The PyMOL Molecular Graphics System*, DeLano Scientific, San Carlos, CA, USA, **2002**.

Received: June 17, 2011
Published Online: September 12, 2011

  